HHS Public Access

Author manuscript

Eur J Neurosci. Author manuscript; available in PMC 2016 May 01.

Published in final edited form as:

Eur J Neurosci. 2015 May ; 41(10): 1381–1391. doi:10.1111/ejn.12909.

Genetic deletion of the PGE_2 EP3 receptor improves anatomical and functional outcomes after intracerebral hemorrhage

Jenna L Leclerc[1,2], **Andrew S Lampert**[1], **Matthew A Diller**[1], and **Sylvain Doré**[1,2,3,*]

[1]Department of Anesthesiology, University of Florida, Gainesville, FL, USA

[2]Department of Neuroscience, University of Florida, Gainesville, FL, USA

[3]Departments of Neurology, Psychiatry, and Pharmaceutics, University of Florida, Gainesville, FL, USA

Abstract

Intracerebral hemorrhage (ICH) is a stroke subtype associated with high mortality and morbidity. Following ICH, excitotoxicity and inflammation significantly contribute to secondary brain injury and poor outcomes. Prostaglandin E_2 (PGE_2) levels rise locally with insult to the nervous system, and PGE_2 is known to modulate these processes mainly through its E prostanoid (EP) receptors, EP1–4. EP3 is the most abundant EP receptor in the brain and we have previously shown that signaling through the PGE_2-EP3 axis exacerbates excitotoxicity and ischemic stroke outcomes. This study aimed to investigate the contribution of this pathway in modulating anatomical outcomes and functional recovery following ICH. Genetic deletion of the EP3 receptor resulted in 48.2 ± 7.3% less ICH-induced brain injury ($p < 0.005$) and improved functional recovery ($p < 0.05$), as identified by neurological deficit scoring. To start investigating the mechanisms involved in neuroprotection with impaired PGE_2-EP3 signaling, histological staining was performed to evaluate blood and ferric iron accumulation, neuroinflammation, blood brain barrier dysfunction, and peripheral neutrophil infiltration. After ICH, $EP3^{-/-}$ mice demonstrated 49.5 ± 8.8% and 42.8 ± 13.1% less blood ($p < 0.01$) and ferric iron content ($p < 0.05$), respectively. Furthermore, $EP3^{-/-}$ mice had significantly reduced astrogliosis, microglial activation, blood brain barrier breakdown, and neutrophil infiltration. Collectively, these results suggest an injurious role for the PGE_2-EP3 signaling axis in modulating brain injury, inflammation, and neurologic functional recovery after ICH. Modulation of the PGE_2-EP3 signaling axis may represent a putative therapeutic avenue for the treatment of ICH.

Keywords

gliosis; iron; neuroinflammation; neuroprotection; stroke

*Correspondence: Dr. Sylvain Doré, University of Florida, 1275 Center Drive, Gainesville, FL 32610-0159; Phone: 352-273-9663; sdore@ufl.edu.

The authors declare that they have no competing interests.

Introduction

Intracerebral hemorrhage (ICH) is a devastating stroke subtype with no effective treatments (Sahni & Weinberger, 2007; Mayer *et al.*, 2008; Rincon & Mayer, 2008; Crandall *et al.*, 2011). Excitotoxicity and inflammatory processes initiated by the presence of blood components play a significant role in the pathogenesis and outcomes of ICH, causing secondary oxidative brain injury, cell death, and irreversible neurological deficits (Chen & Regan, 2007; Wang & Doré, 2007b; Aronowski & Zhao, 2011; Mendez *et al.*, 2013). Prostaglandin E_2 (PGE_2) is known to modulate these processes in a variety of acute and chronic neurological disorders (Milatovic *et al.*, 2011). After ICH, PGE_2 levels are increased by inflammation-induced expression of cyclooxygenase-2 and microsomal prostaglandin E synthase-1, enzymes that are collectively responsible for PGE_2 formation from arachidonic acid (Gong *et al.*, 2001; Saleem *et al.*, 2009; Ikeda-Matsuo *et al.*, 2010; Wu *et al.*, 2011).

PGE_2 is a potent bioactive lipid with many functions, which can be both synergistic or antagonistic, and neurotoxic or neuroprotective (Ahmad *et al.*, 2006b; Ahmad *et al.*, 2007; Milatovic *et al.*, 2011). The diverse roles of PGE_2 result mainly from its ability to bind multiple E prostanoid (EP) receptors, EP1–4, each differing in their downstream signaling pathways. Adding to the complexity, these EP receptors have varied expression profiles, cellular localization, ligand binding affinities, and desensitization kinetics (Candelario-Jalil *et al.*, 2005; Andreasson, 2010; Milatovic *et al.*, 2011). In the present study, we focus on the EP3 receptor, which undergoes differential splicing yielding multiple isoforms with different carboxy-termini that are able to couple to several G proteins, resulting in varied isoform-dependent signal transduction pathways (Hatae *et al.*, 2002). In mice, three isoforms exist: EP3α, EP3β, and EP3γ (Irie *et al.*, 1993; Sugimoto *et al.*, 1993). Stimulation of these isoforms can result in changes to cyclic adenosine monophosphate (cAMP) levels, calcium mobilization, activation of phospholipase C, and/or activation of rho kinase (Katoh *et al.*, 1996; Narumiya *et al.*, 1999; Hatae *et al.*, 2002; Shum *et al.*, 2003; Ahmad *et al.*, 2007; Ikeda-Matsuo *et al.*, 2010). Thus, target cells can exhibit a wide range of responses as a result of activation of the PGE_2-EP3 signaling axis.

The contribution of PGE_2-EP3 signaling in mediating Alzheimer disease (AD) and ischemic stroke outcomes has been studied using genetic and pharmacologic approaches and *in vitro* and *in vivo* models (Ahmad *et al.*, 2007; Saleem *et al.*, 2009; Ikeda-Matsuo *et al.*, 2010; Ikeda-Matsuo *et al.*, 2011). We, and others, have shown the beneficial effects of EP3 receptor deletion in an oxygen-glucose deprivation-induced *in vitro* model of brain ischemia, and in the transient focal ischemia and N-methyl-D-aspartate-induced excitotoxicity *in vivo* models (Ahmad *et al.*, 2007; Saleem *et al.*, 2009; Ikeda-Matsuo *et al.*, 2011). Likewise, in our other experiments, intracerebroventricular administration of ONO-AE-248, an EP3 receptor agonist, aggravated outcomes in these same two *in vivo* models (Ahmad *et al.*, 2007). Ikeda-Matsuo *et al.* provided additional evidence suggesting improved outcomes in the transient focal ischemia model with systemic administration of ONO-AE3-240, an EP3 antagonist (Ikeda-Matsuo *et al.*, 2011). Ikeda-Matsuo *et al.* further showed that EP3-mediated augmentation of excitotoxicity in an *in vitro* model was ameliorated by the Rho kinase inhibitor Y-27632 (Ikeda-Matsuo *et al.*, 2010; Jeon *et al.*, 2013). In an *in vitro* model of β-amyloid-induced neuroinflammation, and in an *in vivo* model of familial

AD, EP3 receptor deletion reduced proinflammatory gene expression and oxidative stress, and improved outcomes (Shi *et al.*, 2012). Together, these studies suggest a deleterious role for the PGE_2-EP3 signaling axis in modulating outcomes of neurological disorders associated with excitotoxicity and inflammatory components.

Given that ICH is associated with excitotoxicity and strong neuroinflammatory processes, we hypothesized that PGE_2-EP3 signaling would aggravate anatomical and functional outcomes. The present study was designed to evaluate these outcomes, and characterize ferric iron accumulation, gliosis, blood brain barrier breakdown, and neutrophil infiltration following ICH in mice with genetic deletion of the EP3 receptor.

Materials and methods

Mice

All animal protocols were approved by the Institutional Animal Care and Use Committee at the University of Florida and conducted in accordance with guidelines established by the National Institutes of Health. Studies were performed on 2.5 – 4.5 month old male wildtype (WT, 3.2 ± 0.8 months) and EP3 receptor knockout ($EP3^{-/-}$, 4.1 ± 0.4 months) C57BL/6 mice. Colonies were bred and maintained in our animal facilities in a temperature-controlled environment (23 ± 2°C) on a 12 h reverse dark/light cycle so behavioral testing could be performed during the awaken phase. Mice were allowed *ad libitum* access to food and water before and after surgical procedures.

ICH model

ICH was induced in WT (n = 8) and $EP3^{-/-}$ (n = 11) mice using a modified previously described method (Chen *et al.*, 2011; Singh *et al.*, 2013). Additional changes were incorporated in order to avoid needle insertion through the motor cortex, and thus the possibility of confounding results on behavioral analyses and to improve the modeling of clinical deep basal ganglia hemorrhages, where concomitant intraventricular hemorrhage (IVH) is seen in 40% of nontraumatic ICH cases and is associated with poor long-term prognosis (Moradiya *et al.*, 2014; Poon *et al.*, 2014). Changes were accomplished by modifying the site and angle of craniotomy/needle insertion and the site of injection within the striatum. Briefly, stereotactic equipment was first manipulated so the injection could be performed into the left hemisphere at a 40° angle from the vertical plane. Mice were anesthetized using isoflurane (4% induction, 1.5–2% maintenance) and immobilized on a stereotactic frame (Stoelting, Wood Dale, IL). A small left-sided incision in the skin overlying the skull was made in a coronal plane midway between the left eye and ear. A craniotomy was performed at an angle matching that of the stereotactic angle, at the following coordinates: 0.0 mm anteroposterior and 3.8 mm left, relative to bregma. A syringe with a 26 gauge needle (Hamilton Co., Reno, NV) was inserted 3.6 mm ventral from the skull surface and 0.04 units of collagenase type VII-S (Sigma, St. Louis, MO) dissolved in 0.40 μl of sterile water was infused at 0.20 μl/min using an automated injector (Stoelting). The needle was left in place for 5 min and then slowly removed over a 15 min period. Rectal temperatures were maintained at 37.0 ± 0.5°C throughout all surgical procedures and mice

were allowed to fully recover in temperature and humidity-controlled chambers post-operatively.

Determination of initial hemorrhage volume

Since different initial hemorrhage volumes in WT and EP3$^{-/-}$ mice could influence anatomical and functional outcomes, we assessed brain hemoglobin content in both groups at the point of maximal bleeding, 5 h post-surgery, as we have described (Wang & Doré, 2007a). Briefly, WT (n = 3) and EP3$^{-/-}$ (n = 4) mice were deeply anesthetized and transcardially perfused with phosphate-buffered saline (PBS, pH 7.4). After quick removal of the brain, the olfactory bulbs and cerebellum were discarded and the ipsilateral and contralateral hemispheres were separately snap frozen in 2-methylbutane pre-cooled over dry ice. Samples were thawed and homogenized for 5 min in 700 μl of sterile deionized water. After centrifugation at 14,000 rpm and 4°C for 30 min, the supernatant was used for hemoglobin determination by Drabkin's method (Sigma). An eight point standard curve was generated by spiking 15 μl of lysed citrate anti-coagulated blood, collected by intracardial puncture from control animals, into 135 μl of a pooled contralateral hemisphere supernatant with two-fold dilutions thereafter. In a 96 well plate, 50 μl of Drabkin's reagent was added to 50 μl of supernatant. All samples were run in triplicate. After 15 min incubation at room temperature, cyanomethemoglobin concentration, reflecting brain hemoglobin content and thus initial hemorrhage volume, was determined by absorbance at 540 nm.

Functional outcomes

Functional outcomes were assessed daily post-ICH by neurological deficit scoring (NDS), accelerating rotarod performance, and open field locomotor activity. Testing was performed during the dark cycle (awaken phase) by investigators blinded to genotype. Each test was performed at the same time of the day and mice were allowed 1 h of rest in between tests. NDS: two blinded investigators independently assessed mice for focal neurological deficits as we have described previously (Glushakov *et al.*, 2013). Briefly, a score of 0 (no deficits) to 4 (severe deficits) was assigned for six individual parameters including body symmetry, gait, circling behavior, climbing, front limb symmetry, and compulsory circling. The average of the sum of the individual scores for the two investigators is reported as NDS. Accelerating rotarod performance: mice were evaluated for motor deficits and coordination, endurance, and balance using an accelerating rotarod Rotamex-5 machine and software (Columbus, OH). Rotational speed started at 4 rpm and ended at 30 rpm, and the latency to fall was automatically collected by the software. On the three consecutive days prior to surgery, mice were trained twice per day (morning and late afternoon) with three cycles per training period. Average performance on the sixth training period served as baseline functioning. Post-ICH testing consisted of one testing period per day with three cycles and data is reported as the average latency to fall. Open field locomotor activity: ambulatory distance and stereotypic time was measured using an automated open field activity monitor and video tracking interface system (MED associates, St. Albans, VT). In this context, stereotypic behavior represents fine motor ability defined as any movement confined within a 4.8 × 4.8 cm space relative to the mouse center point. Baseline locomotor activity was assessed the day prior to surgery, before rotarod training and pre-testing. For baseline and post-ICH testing, mice were placed individually in 4 transparent acrylic cages and their

locomotor activity was recorded over a 30 min period. The first 5 min of recorded data was omitted to exclude for initial anxiety responses.

Histology

At 72 h post-ICH, mice were deeply anesthetized and transcardially perfused with PBS followed by 4% paraformaldehyde. Brains were collected and kept in 4% paraformaldehyde for at least 24 h prior to cryopreservation in a 30% sucrose/PBS solution. Ten sets of sixteen sections equally distributed throughout the entire hematoma and anteroposterior brain regions were processed on a Leica CM 1850 cryostat at 30 μm and stored at −80°C for later histological procedures. In this way, for each animal, multiple staining procedures can be performed and the staining pattern throughout the whole brain can be analyzed. Cresyl violet staining was used to assess lesion volume, ipsilateral hemispheric enlargement, blood accumulation, and the incidence of IVH (Ahmad *et al.*, 2006a). To estimate ferric iron content, Perls' iron stain was completed by incubating slides in a 1:1 mix of 2% hydrochloric acid and 2% potassium ferrocyanide for 20 min, followed by counterstaining with nuclear fast red. Immunohistochemistry was performed to evaluate microgliosis, astrogliosis, blood brain barrier (BBB) breakdown, and neutrophil infiltration using the following primary antibodies: ionized calcium-binding adapter protein 1 (Iba1), 1:1000 (01919741, Wako, Richmond, VA); glial fibrillary acidic protein (GFAP), 1:1000 (Z033429-2, Dako, Carpinteria, CA); immunoglobulin G (IgG), 1:300 (BA-2000, Vector Laboratories, Burlingame, CA); and myeloperoxidase (MPO), 1:500 (PA5-16672, Pierce, Dallas, TX), respectively. Briefly, slides were washed three times in PBS and subsequently incubated in a 1.5% hydrogen peroxide solution diluted in methanol for 30 min. After three additional washes, slides were incubated in a blocking/permeabilization buffer consisting of 10% horse serum and 0.3% Triton X-100 in PBS for 1 h. Then, primary antibodies diluted in 2% horse serum and 0.3% Triton X-100 in PBS were added and slides were left overnight at 4°C. The following day, slides were washed and incubated in secondary antibody diluted in the same buffer as was used for the primary antibody. A secondary biotinylated anti-rabbit antibody was used for detection (BA-1100, Vector Laboratories), except for in the case of IgG staining, which used a secondary biotinylated anti-mouse IgG antibody as the primary antibody (single day staining procedure). After an additional three washes, the Vectastain Elite ABC kit PK-6100 and DAB kit SK-4100 (Vector Laboratories) were used per manufacturer's instructions for the avidin/biotin-peroxidase step and final DAB reaction, respectively. MPO and IgG slides were counterstained with Cresyl Violet, while GFAP and Iba1 slides were not counterstained. After Cresyl violet, Perls' iron and immunohistochemistry, slides were dehydrated in increasing concentrations of ethanol and coverslipped with Permount.

Quantification procedures

All slides were scanned using a ScanScope CS (Aperio Technologies, Inc., Vista, CA) and analyzed with ImageScope software (Aperio Technologies). Quantification was performed in a blinded manner and to reduce any potential bias and inter-individual variability, for a given histological stain, all slides simultaneously underwent the staining protocol and a single investigator performed the quantification. For quantification procedures in which total brain pathology was analyzed (lesion volume, ipsilateral hemispheric enlargement, blood

accumulation, ferric iron content, BBB breakdown, and peripheral neutrophil infiltration), all 16 sections were quantified for each animal. To assess astrogliosis and microgliosis, the same four sections for each animal representing maximal lesion area were analyzed. Lesion volume: injured brain regions were outlined, areas abstracted from the ImageScope software, and a volume was calculated using these areas, known distance between each section, and section thickness. Percent ipsilateral hemispheric enlargement: the whole brain and contralateral hemisphere were outlined, volumes were determined as described above, and the percent ipsilateral hemispheric enlargement was calculated by 100*[(ipsilateral-contralateral)/contralateral]. IVH: the visual presence of red blood cells within the lateral ventricles was counted as IVH. Blood accumulation, ferric iron content and immunohistochemical stains: the ImageScope 'Positive Pixel Count' algorithm was used for quantification after the appropriate brain regions were outlined (see below). Algorithms were tuned for each of the stains such that the appropriate signal and strength of signal was evaluated and detailed supplementary methods are provided in the supporting information (available online). Cortical microgliosis was analyzed by placing identically sized boxes of 1000 by 1000 pixels in the ipsilateral and contralateral motor cortex. Data are presented as the relative ipsilateral to contralateral signal. Striatal microgliosis was analyzed by outlining of the ipsilateral and contralateral striatum, excluding the lesion area. Data are presented as the ipsilateral signal per area quantified, with normalization for the contralateral signal per area quantified. Cortical and striatal astrogliosis were analyzed in a similar manner to microgliosis; however, these data were not normalized for the contralateral equivalent due to negligible signal in the contralateral cortex and striatum with the algorithm thresholds and signal intensity used in the quantification procedures (see supporting information). Blood accumulation, ferric iron content and MPO slides were analyzed by circling of the ipsilateral hemisphere. Whole brain signal was examined for IgG quantification since staining extended into the contralateral side in some cases. After all analyses, the appropriate algorithm was run and signal data was abstracted from the ImageScope software.

Statistics

GraphPad Prism 6 software was used for all statistical analyses (San Diego, CA). Differences between two groups were determined by an unpaired two-tailed parametric Student's t-test. The incidence rate for IVH was compared using Fisher's exact test. Behavioral data was analyzed using a parametric repeated measures two-way ANOVA and Newman-Keuls multiple comparisons test, except for NDS, which was analyzed within groups using a nonparametric repeated measures one-way ANOVA Friedman test. Data are expressed as mean ± SEM, and $p < 0.05$ was considered statistically significant in all analyses.

Results

Consistent striatal hemorrhages were seen in both WT and $EP3^{-/-}$ mice and no significant differences in percent body weight loss was seen between the groups at any time point post-ICH. Mortality rates for the WT and $EP3^{-/-}$ mice were 12.5% and 18.2%, respectively. Histological staining and neurobehavioral testing were performed to evaluate various anatomical and functional outcomes, respectively.

Deletion of the PGE_2 EP3 receptor attenuates ICH-induced brain injury

When compared to WT controls, $EP3^{-/-}$ mice displayed significantly smaller lesions with less blood accumulation (Fig. 1A). Quantification of lesion volume showed that $EP3^{-/-}$ mice had 48.2 ± 7.3% smaller lesions when compared to WT controls (9.3 ± 1.3 mm^3 vs. 17.8 ± 2.0 mm^3, p = 0.0027; Fig. 1B). Analysis of red/brown positive pixel count demonstrated that $EP3^{-/-}$ mice had 49.5 ± 8.8% less blood accumulation (2.9 ± 0.5 × 10^7 A.U. vs. 5.7 ± 0.8 × 10^7 A.U., p = 0.0073; Fig. 1C). No significant differences in percent ipsilateral hemispheric enlargement were seen between the groups (10.9 ± 1.8% vs. 13.5 ± 2.4%, p = 0.3789; Fig. 1D). The overall rate of IVH was 60%, although $EP3^{-/-}$ mice had a significantly decreased incidence of IVH when compared to WT controls (25% vs. 100%, p = 0.0070).

EP3 receptor deletion has no effect on initial hemorrhage volume

Brain hemoglobin content was measured at the point of maximal collagenase-induced bleeding to determine whether differences in initial hemorrhage volumes were responsible for the improved anatomical outcomes and functional recovery seen in $EP3^{-/-}$ mice. Hemoglobin levels were not significantly different between WT and $EP3^{-/-}$ mice ($EP3^{-/-}$: 0.097 ± 0.005 A.U., WT: 0.102 ± 0.011 A.U., p = 0.6677), indicating that initial hemorrhage volumes were the same for the two genotypes.

Effect of PGE_2 EP3 receptor deletion on functional outcomes after ICH

Neurobehavioral testing was performed at 24, 48, and 72 h after ICH by investigators blinded to genotype. When comparing WT and $EP3^{-/-}$ groups, we did not find significant differences on NDS, accelerating rotarod performance, or open field locomotor activity. Deletion of the EP3 receptor did not affect baseline open field locomotor activity, however, $EP3^{-/-}$ mice had a reduced baseline latency to fall on an accelerating rotarod ($p < 0.01$). At all time points post-ICH, WT and $EP3^{-/-}$ mice had significantly reduced ambulatory and stereotypic movements, and worse rotarod performance when compared to baseline function ($p < 0.0001$). As identified by NDS, $EP3^{-/-}$ mice demonstrated improved neurological recovery after ICH ($p < 0.05$), whereas no such improvements were seen for the WT mice (Fig. 2A). Neither group displayed recovery in rotarod performance at any time point post-ICH (Fig. 2B). WT and $EP3^{-/-}$ mice had similar open field locomotor activity, where significant improvements in ambulatory distance were seen at 72 h when compared to 24 h ($p < 0.0001$ for both WT and $EP3^{-/-}$ mice) and 48 h (WT: $p < 0.01$, $EP3^{-/-}$: $p < 0.001$), while no differences were seen between 24 and 48 h (Fig. 2C). Likewise, both groups had significant recovery in stereotypic time at 72 h after ICH when compared to 24 h (WT: $p < 0.01$, $EP3^{-/-}$: $p < 0.0001$; Fig. 2D), but only $EP3^{-/-}$ mice demonstrated improvements at 72 h when compared to 48 h functioning ($p < 0.001$; Fig. 2D). No significant differences in stereotypic time were seen for either group between 24 and 48 h (Fig. 2D). These results indicate that more post-ICH recovery in locomotor activity occurs within the 48 to 72 h period, particularly in the $EP3^{-/-}$ mice, with less recovery between 24 and 48 h.

Deletion of the PGE_2 EP3 receptor reduces brain ferric iron content after ICH

To begin identifying the mechanisms involved in EP3-mediated neurotoxicity after ICH, Perls' iron staining was performed to assess brain ferric iron content. Ferric iron deposition

(blue) was primarily localized to perihematomal regions in both WT and EP3$^{-/-}$ mice (Fig. 3A). Analysis of blue positive pixel count showed that EP3$^{-/-}$ mice had 42.8 ± 13.1% less ferric iron in the ipsilateral hemisphere when compared to WT controls (3.0 ± 0.7 × 10^5 A.U. vs. 5.2 ± 0.8 × 10^5 A.U., p = 0.0488, Fig. 3B). No Perls' staining was seen in the contralateral hemisphere for any of the mice in the study.

Effect of PGE_2 EP3 receptor deletion on gliosis after ICH

To further delineate mechanisms, immunohistochemistry for Iba1 and GFAP was performed to assess cortical and striatal microgliosis and astrogliosis, respectively. Following ICH, EP3$^{-/-}$ mice displayed less striatal microglial activation and morphological changes when compared to WT controls, whereas no significant difference was seen in cortical microgliosis. In both groups, significantly increased microglial activation and morphological changes were noted in the ipsilateral cortex (Fig. 4A) and striatum (Fig. 4B) compared to the contralateral equivalent areas. No significant differences in microglial activation or morphological changes were seen between the two groups in the contralateral striatum or cortex. After quantification, WT and EP3$^{-/-}$ mice showed similar cortical microgliosis (EP3$^{-/-}$: 2.8 ± 0.5 A.U., WT: 3.0 ± 0.4 A.U., p = 0.7725, Fig. 4C). However, EP3$^{-/-}$ mice had 57.7 ± 11.0% less striatal microgliosis when compared to WT controls (2.7 ± 0.3 A.U. vs. 8.4 ± 2.5 A.U., p = 0.0599, Fig. 4D). The increased ipsilateral activation and morphological changes were considerably more pronounced in the striatum when compared to the cortex for the WT group (p = 0.0491), whereas no significant difference was seen for the EP3$^{-/-}$ mice (p = 0.2057).

When compared to WT controls, the EP3$^{-/-}$ mice had significantly less cortical astrogliosis, and tended to have reduced striatal astrogliosis. In both groups, significantly increased astrogliosis was noted in the ipsilateral cortex (Fig. 5A) and striatum (Fig. 5B) compared to the contralateral equivalent areas. After quantification, EP3$^{-/-}$ mice had 54.2 ± 8.4% less cortical astrogliosis (0.0213 ± 0.0039 A.U. vs. 0.0465 ± 0.0112 A.U., p = 0.0429, Fig. 5C). Similarly, EP3$^{-/-}$ mice tended to have 33.0 ± 12.0% less striatal astrogliosis (0.0362 ± 0.0065 A.U. vs. 0.0540 ± 0.0083 A.U., p = 0.1102, Fig. 5D). Ipsilateral cortical and striatal astrogliosis were similar for WT mice (p = 0.5977), but EP3$^{-/-}$ mice tended to have more striatal astrogliosis compared to cortical (p = 0.0681).

Deletion of the PGE_2 EP3 receptor reduces peripheral neutrophil infiltration after ICH

Additionally, infiltration of neutrophils from the periphery was evaluated by immunohistochemical staining for MPO, a major constituent of neutrophil azurophilic granules. MPO+ cells (brown) were diffusely localized within the hematoma, with occasional focal sites of concentration surrounding blood vessels (Fig. 6A). No MPO+ cells were seen outside of the injured brain regions for any of the mice in the study. Brown positive pixel count analysis showed that EP3$^{-/-}$ mice had 55.3 ± 9.6% less neutrophil infiltration when compared to WT controls (1.6 ± 0.3 × 10^5 A.U. vs. 3.6 ± 0.8 × 10^5 A.U., p = 0.0203, Fig. 6B).

Deletion of the PGE_2 EP3 receptor attenuates blood brain barrier breakdown after ICH

Lastly, BBB breakdown was evaluated by immunohistochemical staining for mouse IgG. WT mice displayed increased disruption of the BBB with a more diffuse staining pattern when compared to $EP3^{-/-}$ mice (Fig. 7A). Brown positive pixel count analysis showed that $EP3^{-/-}$ mice had 37.3 ± 14.2% less BBB breakdown when compared to WT controls (2.5 ± 0.4 × 10^{10} A.U. vs. 5.0 ± 0.5 × 10^{10} A.U., p = 0.0020, Fig. 7B).

Discussion

In the present study, we have investigated the role of the PGE_2-EP3 signaling axis in modulating anatomical and functional outcomes after ICH. Genetic deletion of the EP3 receptor resulted in less ICH-induced brain injury evident by smaller lesion volumes with reduced blood and ferric iron accumulation and less incidence of IVH. No significant differences in neurological function were seen when comparing WT and $EP3^{-/-}$ mice at the same time point post-ICH with the behavioral tests utilized here; however, $EP3^{-/-}$ mice did show better recovery with NDS. Improved anatomical and functional recovery in $EP3^{-/-}$ mice was accompanied by less cortical and striatal astrogliosis, striatal microgliosis, BBB breakdown, and peripheral neutrophil infiltration. Collectively, these results imply an injurious role for signaling through the PGE_2-EP3 pathway after ICH.

The EP3 receptor is reported to be the most abundantly expressed E prostanoid receptor subtype in the brain (Sugimoto *et al.*, 1994; Nakamura *et al.*, 2000), is involved in many important physiological functions and pathological conditions of the nervous system, and after insult, expression is induced in cells uniquely situated to modulate outcomes. Furthermore, formation of PGE_2 is similarly increased under these pathological conditions (Gong *et al.*, 2001; Ikeda-Matsuo *et al.*, 2010; Wu *et al.*, 2011), suggesting an important role for the PGE_2-EP3 signaling axis. Physiologically, EP3 has been shown to be important in fever induction, pain modulation, and regulation of the autonomic nervous system (Mantelli *et al.*, 1991; Kumazawa *et al.*, 1993; Minami *et al.*, 1994; Yokotani *et al.*, 1996; Ushikubi *et al.*, 1998). A few studies have characterized EP3 receptor expression and localization and regions of the brain associated with these physiologic functions express high levels of the receptor. Under normal conditions, EP3 is constitutively expressed predominately in neurons of the cerebral cortex, striatum, thalamus, hypothalamus, substantia nigra, hippocampus, locus coeruleus, raphe nuclei, and periaqueductal grey, among a few other places (Sugimoto *et al.*, 1994; Nakamura *et al.*, 2000). Pathologically, EP3 expression was induced in macrophages/microglia neighboring the lesion in models of excitotoxicity and transient focal ischemia (Slawik *et al.*, 2004; Ikeda-Matsuo *et al.*, 2011). Astrocytic EP3 expression is controversial and probably pathology-dependent, but expression has been shown *in vivo* after kainic acid or IL-1β treatment (Sugimoto *et al.*, 1994; Kitanaka *et al.*, 1996; Caggiano & Kraig, 1999; Slawik *et al.*, 2004; Takemiya *et al.*, 2010; Shi *et al.*, 2012). Therefore, under basal conditions, EP3 receptor expression is restricted to areas consistent with its physiologic roles in modulation of neuronal function; whereas, with pathological processes, EP3 expression is induced in glia situated in an optimal location to have an important additional contribution in mediating the outcomes of potentially viable cells (i.e. adjacent to the lesion).

Our findings suggesting a deleterious role for the PGE_2-EP3 signaling axis after ICH are in agreement with previous studies investigating the contribution of this pathway under other neuropathological conditions. We and others have shown that signaling through the EP3 receptor exacerbates outcomes in *in vitro* and *in vivo* models of excitotoxicity and brain ischemia (Ahmad *et al.*, 2007; Saleem *et al.*, 2009; Ikeda-Matsuo *et al.*, 2010; Ikeda-Matsuo *et al.*, 2011). Similarly, deletion of the EP3 receptor leads to improved outcomes in a model of AD (Shi *et al.*, 2012). Here, we have shown that $EP3^{-/-}$ mice display smaller lesion volumes associated with less blood and ferric iron accumulation 72 h following ICH. Deletion of the EP3 receptor also resulted in less incidence of IVH, likely resulting from the smaller lesions and less extension of blood into the lateral ventricles. Several possible interconnected mechanisms exist to explain the observed outcomes: 1) deletion of the EP3 receptor alters vascular anatomy, hemostatic competence, and/or susceptibility to collagenase-induced bleeding leading to smaller initial hemorrhage volumes, 2) EP3 signaling exerts a negative modulatory effect on macrophage/microglial phagocytic capability, 3) signaling through the EP3 receptor increases excitotoxic responses, 4) EP3 signaling affects neuroinflammatory processes, and 5) signaling through the EP3 receptor increases secondary BBB dysfunction. Differences in collagenase-induced bleeding tendency with EP3 receptor deletion is unlikely since $EP3^{-/-}$ mice have been reported to not have differences in vascular anatomy (Ikeda-Matsuo *et al.*, 2011) and we have provided evidence showing equivalent initial hemorrhage volumes for the two genotypes. Furthermore, selective antagonism of the EP3 receptor does not affect hemostatic competence (Singh *et al.*, 2009; Tilly *et al.*, 2014), corroborating the similar total hemoglobin levels seen here, and suggesting that deletion of the EP3 receptor would not influence the hematoma distribution and resulting differential compression of surrounding brain tissue. To our knowledge, an EP3-mediated modulatory effect on phagocytosis has not been described (as is the case with other EP receptor subtypes); thus, we cannot exclude this potential mechanism as a contributing factor in the current study. Early PGE_2-EP3-mediated excitotoxicity and neuroinflammatory responses could lead to secondary BBB dysfunction and leakage of additional blood components, which would then augment the inflammatory responses to the primary bleed, further exacerbating outcomes in WT mice. Alternatively, a direct local PGE_2-EP3-mediated negative modulation of BBB integrity could also explain the observed outcomes. It appears that the structural organization is in place for such a direct role, as brain endothelial cells and astrocyte end feet were shown to produce PGE_2 and express EP3, respectively, in a kainate-induced excitotoxicity model (Takemiya *et al.*, 2010). Although the exact mechanisms underlying the improved outcomes seen here in $EP3^{-/-}$ mice after ICH are not known, we have shown that deletion of the EP3 receptor results in strong trends towards reduced striatal astrogliosis and microgliosis and significantly reduced cortical astrogliosis, BBB breakdown, and peripheral neutrophil infiltration. The reduced astrogliosis may be indicative of less endothelial-derived toxic PGE_2 signaling and could explain the decreased BBB dysfunction seen in $EP3^{-/-}$ mice. Although, several other possibilities exist including less microglial activation and release of toxic pro-inflammatory cytokines and less neutrophil degranulation and release of proteolytic enzymes, both of which would improve BBB integrity. Broadening of these results to the autologous blood ICH model to address the potential contribution of collagenase-induced inflammatory and/or ischemic responses and incorporating earlier and

later endpoints to determine the sequence of events are necessary additional experiments to clarify the role of the PGE_2-EP3 signaling axis in modulating ICH outcomes and understand the mechanisms involved. Additionally, these studies should include pharmacologic manipulation of the EP3 receptor with the currently available selective agonists and antagonists for confirmation and to ensure minimal contribution from any potential concurrently operating compensatory mechanisms.

At each behavioral testing time point post-ICH, functional outcomes were not significantly different between the WT and $EP3^{-/-}$ mice on any of the tests. The inconsistency between anatomical and functional outcomes could be due to the inherent challenge of detecting subtle changes in neurological function in mice. Moreover, lager differences between groups may exist and be easier to detect at later time points with this ICH model given the extensive damage produced early on; a suggestion that is supported by the severe deficits remaining in both experimental groups at the study endpoint with all three neurobehavioral tests performed. Alternatively, $EP3^{-/-}$ mice may have some confounding baseline differences that negate any potential protective effects after ICH. Indeed, we have shown that $EP3^{-/-}$ mice had a significantly reduced baseline latency to fall on an accelerating rotarod. Nevertheless, less focal neurological deficits were seen for $EP3^{-/-}$ mice at 48 and 72 h when compared to 24 h functioning as identified by NDS; whereas, no such improvement was seen for WT mice, suggesting that deletion of the EP3 receptor improves the rate of functional recovery.

While it seems that PGE_2-EP3 signaling plays a key role in modulating outcomes following insult to the nervous system, the mechanisms and effector molecules downstream of the EP3 receptor are not yet understood. With three EP3 isoforms, likely co-expressed on the same cell, displaying varied PGE_2 binding affinity, ligand-receptor complex affinity for the G protein (Sugimoto *et al.*, 1993), and isoform-dependent signal transduction pathways, the possibilities are multiple and complex. Through coupling to a $G_{\alpha i}$ protein, activation of the EP3α and EP3β isoforms results in inhibition of adenylyl cyclase and decreased cAMP levels; whereas, EP3γ couples to both $G_{\alpha s}$ and $G_{\alpha i}$ proteins and has stimulatory and inhibitory effects on adenylyl cyclase and cAMP production (Sugimoto *et al.*, 1993; Irie *et al.*, 1994; Mohan *et al.*, 2012). However, with respect to cAMP levels, it has been suggested that the net effect of EP3 receptor stimulation is mediated through coupling to $G_{\alpha i}$, resulting in decreased cAMP accumulation (Irie *et al.*, 1994). Activation of all EP3 isoforms has been shown to increase intracellular calcium levels through a G_i-phospholipase C coupling mechanism (Irie *et al.*, 1994). Finally, EP3β activation, but not EP3α1 (human), has been associated with a Rho kinase (ROCK) activation pathway (Katoh *et al.*, 1996; Scott *et al.*, 2007). The contribution of each of these PGE_2-EP3 signaling pathways in modulating outcomes is difficult to delineate since the isoforms are generated by alternative RNA splicing and genetic deletion and pharmacologic manipulation of the EP3 receptor results in global deletion or activation of all isoforms (to different levels due to varied ligand affinity), respectively. Although, the relative balance of isoforms, and thus the “net” signaling pathway, is probably the important factor for determining outcomes; a hypothesis that is supported by the varied responses of tissues to EP3 stimulation that express different relative amounts of these isoforms (Israel & Regan, 2009).

In the context of the current study, with the absence or presence of all EP3 isoforms, each of these downstream pathways could be contributing to the improved ICH outcomes in $EP3^{-/-}$ mice. It is tempting to hypothesize that calcium mobilization is the key contributor since all three isoforms participate in increasing extracellular calcium influx and release from intracellular stores; thus, EP3 signaling would be expected to augment this response, aggravating calcium-mediated neuronal and glial injury. However, we have previously shown that anatomical and functional outcomes were exacerbated with deletion of the EP1 receptor, another G-protein coupled EP receptor that upon stimulation, like EP3, results in activation of phospholipase C and increased intracellular calcium (Singh *et al.*, 2013). The discrepancy in ICH outcomes, despite a common signaling pathway between EP1 and EP3, suggests that another mechanism is responsible or that the relative contribution of calcium-mediated damage is different upon EP1 or EP3 stimulation after ICH. Alternatively, the cAMP and Rho kinase EP3 signaling pathways (which EP1 does not possess) may play a greater role in arbitrating ICH outcomes. Increased intracellular cAMP elicits numerous cellular survival functions, including neuronal survival, axonal regeneration, and enhancement of neurite outgrowth (Ahmad *et al.*, 2007); thus, with absent EP3 signaling, improved outcomes would be expected, as seen here. However, better ICH outcomes were also seen with deletion of the EP2 receptor, which opposite to EP3, results in G_s-mediated adenylyl cyclase activity and increases in intracellular cAMP levels upon stimulation (under submission). ROCK activation is the least studied downstream pathway of EP3, although PGE_2-EP3-ROCK signaling has been implicated as the mechanism for EP3-mediated neurite retraction, vascular contraction, and importantly, neurotoxic responses following glutamate-induced excitotoxicity (Katoh *et al.*, 1996; Shum *et al.*, 2003; Ikeda-Matsuo *et al.*, 2010; Jeon *et al.*, 2013). Furthermore, the RhoA/ROCK pathway has been reported as the mechanism leading to BBB dysfunction after endothelial activation by thrombin (van Nieuw Amerongen *et al.*, 2008; Posada-Duque *et al.*, 2014). While it is a daunting task, additional studies are needed to more clearly delineate the exact mechanisms involved in neurotoxicity after brain injury with PGE_2-EP3 signaling, including the EP3-expressing cells responsible and relative contribution of each of the isoforms, signaling pathways, and downstream effector molecules, such that improved therapeutics can be developed for various neurological conditions including hemorrhagic stroke.

The present study is the first to investigate the role of the PGE_2-EP3 signaling axis following ICH, where we have provided evidence suggesting an injurious role for this pathway. Deletion of the EP3 receptor led to improved anatomical outcomes and functional recovery after ICH. Specifically, $EP3^{-/-}$ mice demonstrated smaller lesion volumes associated with less blood and ferric iron accumulation, and reduced gliosis, BBB breakdown, and peripheral neutrophil infiltration. The G-protein coupled EP3 receptor may represent a new therapeutic target for the treatment of hemorrhagic stroke.

Supplementary Material

Refer to Web version on PubMed Central for supplementary material.

Acknowledgments

This work was supported by grants from the National Institutes of Health F31NS086441 (JLL) and R01NS046400 (SD). We thank all members of the Doré lab for helpful discussions and technical assistance, with a special acknowledgment of the many talented undergraduate students who contributed to the brain sectioning, immunohistochemical staining and blinded quantification and behavioral procedures.

Abbreviations

ABC	Avidin/biotin enzyme complex
AD	Alzheimer's disease
ANOVA	Analysis of variance
BBB	Blood brain barrier
cAMP	Cyclic adenosine monophosphate
DAB	3,3′-diaminobenzidine
EP3	E prostanoid receptor subtype 3
EP3$^{-/-}$	EP3 receptor knockout
GFAP	Glial fibrillary acidic protein
Iba1	Ionized calcium-binding adapter protein 1
ICH	Intracerebral hemorrhage
IgG	Immunoglobulin G
IVH	Intraventricular hemorrhage
MPO	Myeloperoxidase
NDS	Neurological deficit score
PBS	Phosphate-buffered saline
PGE_2	Prostaglandin E_2
ROCK	Rho kinase
SEM	Standard error of the mean
WT	Wildtype

References

Ahmad AS, Saleem S, Ahmad M, Doré S. Prostaglandin EP1 receptor contributes to excitotoxicity and focal ischemic brain damage. Toxicol Sci. 2006a; 89:265–270. [PubMed: 16237196]

Ahmad M, Ahmad AS, Zhuang H, Maruyama T, Narumiya S, Doré S. Stimulation of prostaglandin E_2-EP3 receptors exacerbates stroke and excitotoxic injury. Journal of neuroimmunology. 2007; 184:172–179. [PubMed: 17275922]

Ahmad M, Saleem S, Zhuang H, Ahmad AS, Echeverria V, Sapirstein A, Doré S. 1-HydroxyPGE$_1$ reduces infarction volume in mouse transient cerebral ischemia. Eur J Neurosci. 2006b; 23:35–42. [PubMed: 16420413]

Andreasson K. Prostaglandin signalling in cerebral ischaemia. British journal of pharmacology. 2010; 160:844–846. [PubMed: 20590583]

Aronowski J, Zhao X. Molecular pathophysiology of cerebral hemorrhage: secondary brain injury. Stroke; a journal of cerebral circulation. 2011; 42:1781–1786.

Caggiano AO, Kraig RP. Prostaglandin E receptor subtypes in cultured rat microglia and their role in reducing lipopolysaccharide-induced interleukin-1beta production. Journal of neurochemistry. 1999; 72:565–575. [PubMed: 9930728]

Candelario-Jalil E, Slawik H, Ridelis I, Waschbisch A, Akundi RS, Hull M, Fiebich BL. Regional Distribution of the Prostaglandin E2 Receptor EP1 in the Rat Brain: Accumulation in Purkinje Cells of the Cerebellum. J Mol Neurosci. 2005; 27:303–310. [PubMed: 16280600]

Chen L, Zhang X, Chen-Roetling J, Regan RF. Increased striatal injury and behavioral deficits after intracerebral hemorrhage in hemopexin knockout mice. Journal of neurosurgery. 2011; 114:1159–1167. [PubMed: 21128737]

Chen M, Regan RF. Time course of increased heme oxygenase activity and expression after experimental intracerebral hemorrhage: correlation with oxidative injury. Journal of neurochemistry. 2007; 103:2015–2021. [PubMed: 17760860]

Crandall KM, Rost NS, Sheth KN. Prognosis in intracerebral hemorrhage. Reviews in neurological diseases. 2011; 8:23–29. [PubMed: 21769068]

Glushakov AV, Robbins SW, Bracy CL, Narumiya S, Doré S. Prostaglandin F2alpha FP receptor antagonist improves outcomes after experimental traumatic brain injury. Journal of neuroinflammation. 2013; 10:132. [PubMed: 24172576]

Gong C, Ennis SR, Hoff JT, Keep RF. Inducible cyclooxygenase-2 expression after experimental intracerebral hemorrhage. Brain research. 2001; 901:38–46. [PubMed: 11368948]

Hatae N, Sugimoto Y, Ichikawa A. Prostaglandin receptors: advances in the study of EP3 receptor signaling. Journal of biochemistry. 2002; 131:781–784. [PubMed: 12038972]

Ikeda-Matsuo Y, Tanji H, Narumiya S, Sasaki Y. Inhibition of prostaglandin E2 EP3 receptors improves stroke injury via anti-inflammatory and anti-apoptotic mechanisms. Journal of neuroimmunology. 2011; 238:34–43. [PubMed: 21803432]

Ikeda-Matsuo Y, Tanji H, Ota A, Hirayama Y, Uematsu S, Akira S, Sasaki Y. Microsomal prostaglandin E synthase-1 contributes to ischaemic excitotoxicity through prostaglandin E2 EP3 receptors. British journal of pharmacology. 2010; 160:847–859. [PubMed: 20590584]

Irie A, Segi E, Sugimoto Y, Ichikawa A, Negishi M. Mouse prostaglandin E receptor EP3 subtype mediates calcium signals via Gi in cDNA-transfected Chinese hamster ovary cells. Biochem Biophys Res Commun. 1994; 204:303–309. [PubMed: 7945376]

Irie A, Sugimoto Y, Namba T, Harazono A, Honda A, Watabe A, Negishi M, Narumiya S, Ichikawa A. Third isoform of the prostaglandin-E-receptor EP3 subtype with different C-terminal tail coupling to both stimulation and inhibition of adenylate cyclase. Eur J Biochem. 1993; 217:313–318. [PubMed: 8223569]

Israel DD, Regan JW. EP(3) prostanoid receptor isoforms utilize distinct mechanisms to regulate ERK 1/2 activation. Biochimica et biophysica acta. 2009; 1791:238–245. [PubMed: 19416642]

Jeon BT, Jeong EA, Park SY, Son H, Shin HJ, Lee DH, Kim HJ, Kang SS, Cho GJ, Choi WS, Roh GS. The Rho-kinase (ROCK) inhibitor Y-27632 protects against excitotoxicity-induced neuronal death in vivo and in vitro. Neurotoxicity research. 2013; 23:238–248. [PubMed: 22810835]

Katoh H, Negishi M, Ichikawa A. Prostaglandin E receptor EP3 subtype induces neurite retraction via small GTPase Rho. The Journal of biological chemistry. 1996; 271:29780–29784. [PubMed: 8939915]

Kitanaka J, Hashimoto H, Gotoh M, Kondo K, Sakata K, Hirasawa Y, Sawada M, Suzumura A, Marunouchi T, Matsuda T, Baba A. Expression pattern of messenger RNAs for prostanoid receptors in glial cell cultures. Brain research. 1996; 707:282–287. [PubMed: 8919306]

Kumazawa T, Mizumura K, Koda H. Involvement of EP3 subtype of prostaglandin E receptors in PGE2-induced enhancement of the bradykinin response of nociceptors. Brain research. 1993; 632:321–324. [PubMed: 8149238]

Mantelli L, Amerini S, Rubino A, Ledda F. Prejunctional prostanoid receptors on cardiac adrenergic terminals belong to the EP3 subtype. British journal of pharmacology. 1991; 102:573–576. [PubMed: 1364821]

Mayer SA, Brun NC, Begtrup K, Broderick J, Davis S, Diringer MN, Skolnick BE, Steiner T, Investigators FT. Efficacy and safety of recombinant activated factor VII for acute intracerebral hemorrhage. The New England journal of medicine. 2008; 358:2127–2137. [PubMed: 18480205]

Mendez NV, Wharton JA, Leclerc JL, Blackburn SL, Douglas-Escobar MV, Weiss MD, Seubert CN, Doré S. Clinical Implications of Bilirubin-Associated Neuroprotection and Neurotoxicity. Int J of Clin Anesthesiol. 2013; 1:1013.

Milatovic D, Montine TJ, Aschner M. Prostanoid signaling: dual role for prostaglandin E2 in neurotoxicity. Neurotoxicology. 2011; 32:312–319. [PubMed: 21376752]

Minami T, Nishihara I, Uda R, Ito S, Hyodo M, Hayaishi O. Characterization of EP-receptor subtypes involved in allodynia and hyperalgesia induced by intrathecal administration of prostaglandin E2 to mice. British journal of pharmacology. 1994; 112:735–740. [PubMed: 7921597]

Mohan S, Ahmad AS, Glushakov AV, Chambers C, Dore S. Putative role of prostaglandin receptor in intracerebral hemorrhage. Front Neurol. 2012; 3:145. [PubMed: 23097645]

Moradiya Y, Murthy SB, Newman-Toker DE, Hanley DF, Ziai WC. Intraventricular thrombolysis in intracerebral hemorrhage requiring ventriculostomy: a decade-long real-world experience. Stroke; a journal of cerebral circulation. 2014; 45:2629–2635.

Nakamura K, Kaneko T, Yamashita Y, Hasegawa H, Katoh H, Negishi M. Immunohistochemical localization of prostaglandin EP3 receptor in the rat nervous system. J Comp Neurol. 2000; 421:543–569. [PubMed: 10842213]

Narumiya S, Sugimoto Y, Ushikubi F. Prostanoid receptors: structures, properties, and functions. Physiological reviews. 1999; 79:1193–1226. [PubMed: 10508233]

Poon MT, Fonville AF, Al-Shahi Salman R. Long-term prognosis after intracerebral haemorrhage: systematic review and meta-analysis. Journal of neurology, neurosurgery, and psychiatry. 2014; 85:660–667.

Posada-Duque RA, Barreto GE, Cardona-Gomez GP. Protection after stroke: cellular effectors of neurovascular unit integrity. Frontiers in cellular neuroscience. 2014; 8:231. [PubMed: 25177270]

Rincon F, Mayer SA. Clinical review: Critical care management of spontaneous intracerebral hemorrhage. Critical care. 2008; 12:237. [PubMed: 19108704]

Sahni R, Weinberger J. Management of intracerebral hemorrhage. Vasc Health Risk Manag. 2007; 3:701–709. [PubMed: 18078021]

Saleem S, Kim YT, Maruyama T, Narumiya S, Doré S. Reduced acute brain injury in PGE2 EP3 receptor-deficient mice after cerebral ischemia. Journal of neuroimmunology. 2009; 208:87–93. [PubMed: 19203800]

Scott G, Fricke A, Fender A, McClelland L, Jacobs S. Prostaglandin E2 regulates melanocyte dendrite formation through activation of PKCzeta. Experimental cell research. 2007; 313:3840–3850. [PubMed: 17850789]

Shi J, Wang Q, Johansson JU, Liang X, Woodling NS, Priyam P, Loui TM, Merchant M, Breyer RM, Montine TJ, Andreasson K. Inflammatory prostaglandin E2 signaling in a mouse model of Alzheimer disease. Annals of neurology. 2012; 72:788–798. [PubMed: 22915243]

Shum WWC, Le GY, Jones RL, Gurney AM, Sasaki Y. Involvement of Rho-kinase in contraction of guinea-pig aorta induced by prostanoid EP3 receptor agonists. British journal of pharmacology. 2003; 139:1449–1461. [PubMed: 12922932]

Singh J, Zeller W, Zhou N, Hategen G, Mishra R, Polozov A, Yu P, Onua E, Zhang J, Zembower D, Kiselyov A, Ramirez JL, Sigthorsson G, Bjornsson JM, Thorsteinsdottir M, Andresson T, Bjarnadottir M, Magnusson O, Fabre JE, Stefansson K, Gurney ME. Antagonists of the EP3 receptor for prostaglandin E2 are novel antiplatelet agents that do not prolong bleeding. ACS chemical biology. 2009; 4:115–126. [PubMed: 19193156]

Singh N, Ma B, Leonardo CC, Ahmad AS, Narumiya S, Doré S. Role of PGE(2) EP1 receptor in intracerebral hemorrhage-induced brain injury. Neurotoxicity research. 2013; 24:549–559. [PubMed: 23824501]

Slawik H, Volk B, Fiebich B, Hull M. Microglial expression of prostaglandin EP3 receptor in excitotoxic lesions in the rat striatum. Neurochemistry international. 2004; 45:653–660. [PubMed: 15234107]

Sugimoto Y, Negishi M, Hayashi Y, Namba T, Honda A, Watabe A, Hirata M, Narumiya S, Ichikawa A. Two isoforms of the EP3 receptor with different carboxyl-terminal domains. Identical ligand binding properties and different coupling properties with Gi proteins. The Journal of biological chemistry. 1993; 268:2712–2718. [PubMed: 8381413]

Sugimoto Y, Shigemoto R, Namba T, Negishi M, Mizuno N, Narumiya S, Ichikawa A. Distribution of the messenger RNA for the prostaglandin E receptor subtype EP3 in the mouse nervous system. Neuroscience. 1994; 62:919–928. [PubMed: 7870313]

Takemiya T, Matsumura K, Sugiura H, Maehara M, Yasuda S, Uematsu S, Akira S, Yamagata K. Endothelial microsomal prostaglandin E synthase-1 exacerbates neuronal loss induced by kainate. J Neurosci Res. 2010; 88:381–390. [PubMed: 19658194]

Tilly P, Charles AL, Ludwig S, Slimani F, Gross S, Meilhac O, Geny B, Stefansson K, Gurney ME, Fabre JE. Blocking the EP3 receptor for PGE2 with DG-041 decreases thrombosis without impairing haemostatic competence. Cardiovascular research. 2014; 101:482–491. [PubMed: 24323317]

Ushikubi F, Segi E, Sugimoto Y, Murata T, Matsuoka T, Kobayashi T, Hizaki H, Tuboi K, Katsuyama M, Ichikawa A, Tanaka T, Yoshida N, Narumiya S. Impaired febrile response in mice lacking the prostaglandin E receptor subtype EP3. Nature. 1998; 395:281–284. [PubMed: 9751056]

van Nieuw Amerongen GP, Musters RJ, Eringa EC, Sipkema P, van Hinsbergh VW. Thrombin-induced endothelial barrier disruption in intact microvessels: role of RhoA/Rho kinase-myosin phosphatase axis. American journal of physiology. Cell physiology. 2008; 294:C1234–1241. [PubMed: 18353893]

Wang J, Doré S. Heme oxygenase-1 exacerbates early brain injury after intracerebral haemorrhage. Brain. 2007a; 130:1643–1652. [PubMed: 17525142]

Wang J, Doré S. Inflammation after intracerebral hemorrhage. Journal of cerebral blood flow and metabolism: official journal of the International Society of Cerebral Blood Flow and Metabolism. 2007b; 27:894–908.

Wu T, Wu H, Wang J, Wang J. Expression and cellular localization of cyclooxygenases and prostaglandin E synthases in the hemorrhagic brain. Journal of neuroinflammation. 2011; 8:22. [PubMed: 21385433]

Yokotani K, Okuma Y, Osumi Y. Inhibition of vagally mediated gastric acid secretion by activation of central prostanoid EP3 receptors in urethane-anaesthetized rats. British journal of pharmacology. 1996; 117:653–656. [PubMed: 8646410]

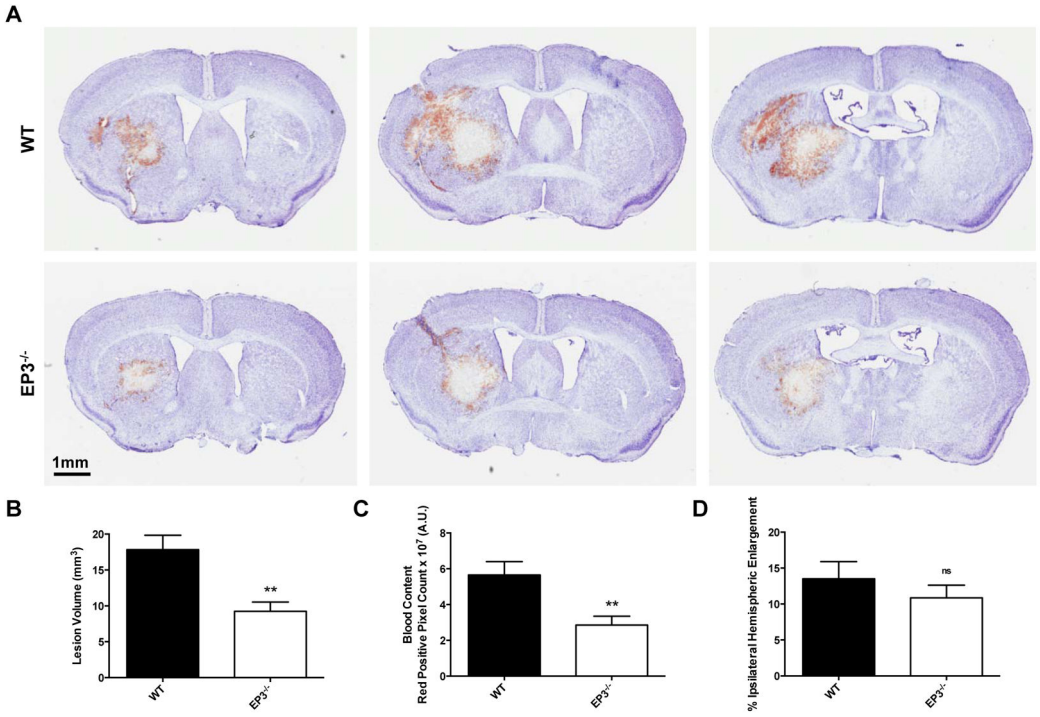

Fig. 1.

Genetic deletion of the PGE_2 EP3 receptor attenuates ICH-induced brain injury. At 72 h after ICH, Cresyl violet staining of coronal brain sections from WT and $EP3^{-/-}$ mice was performed to evaluate brain injury. (A) Representative images showing characteristic hematoma profiles for WT (upper panels) and $EP3^{-/-}$ mice (bottom panels). Images are from the same animal, where left to right corresponds to anterior to posterior and center images are at the needle insertion site, representing maximal brain injury. (B) Lesion volume quantification demonstrated that $EP3^{-/-}$ mice had significantly less brain injury following ICH. (C) Red/brown positive pixel count analysis showed that $EP3^{-/-}$ mice had significantly less blood accumulation within the injured brain areas. (D) No significant difference in percent ipsilateral hemispheric enlargement was seen between the groups. All comparisons included n = 7 WT and n = 8 $EP3^{-/-}$ mice, ns = not significant and $^{**}p < 0.01$.

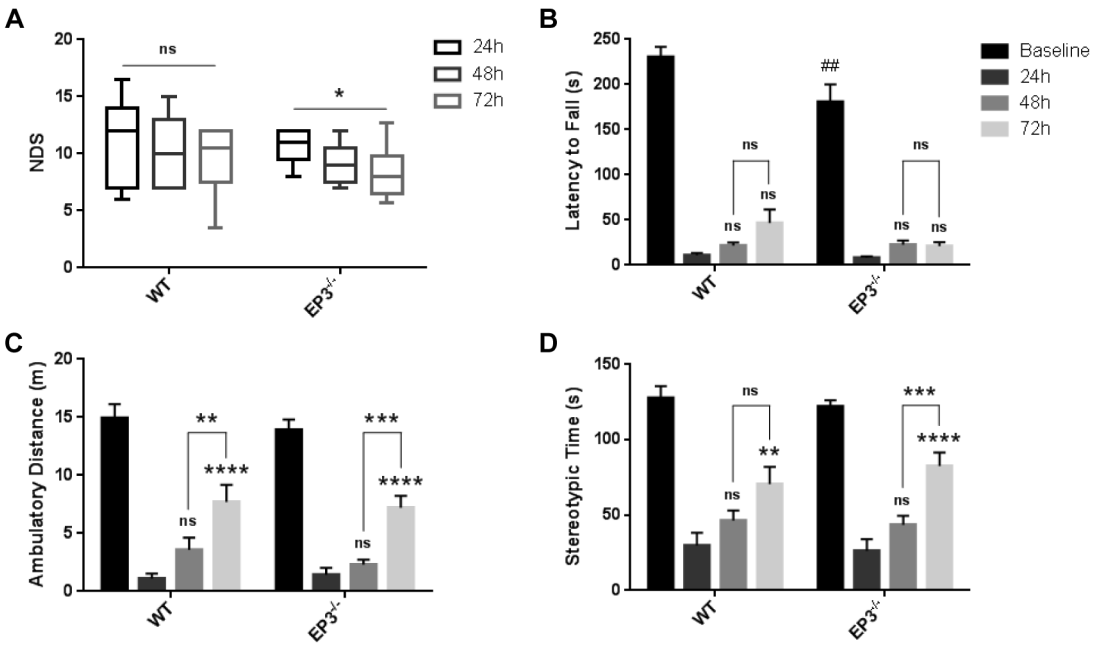

Fig. 2.

Effect of PGE_2 EP3 receptor deletion on functional outcomes after ICH. At 24, 48, and 72 h following ICH, investigators blinded to genotype evaluated the mice for neurological deficits using several neurobehavioral tests. (A) $EP3^{-/-}$ mice had significant improvement in neurological function after ICH as identified by NDS, whereas no such recovery was seen for the WT group. (B) $EP3^{-/-}$ mice performed significantly worse at baseline on an accelerating rotarod. At 24, 48, and 72h after ICH, WT and $EP3^{-/-}$ mice had reduced latency to fall when compared to baseline function ($p < 0.0001$). No recovery in rotarod performance was seen for either group at any time point post-ICH. (C and D) No differences in baseline open field locomotor activity were seen for the WT and $EP3^{-/-}$ mice. Both groups had significantly impaired (C) ambulatory and (D) stereotypic movements at 24, 48, and 72 h post-ICH, when compared to baseline function ($p < 0.0001$). WT and $EP3^{-/-}$ mice had similar open field locomotor activity, where significant improvements in (C) ambulatory distance and (D) stereotypic time were seen at 72 h when compared to 24 h function. Similarly, both groups displayed improvements in (C) ambulatory distance at 72 h when compared to 48 h, but only $EP3^{-/-}$ mice had recovery of (D) stereotypic movements during this time frame. No differences in locomotor activity were seen between 24 and 48 h after ICH for either group. All comparisons included n = 7 WT and n = 9 $EP3^{-/-}$ mice. ns = not significant, *$p < 0.05$, **$p < 0.01$, ***$p < 0.001$, and ****$p < 0.0001$, where the results above bars are with respect to 24 h function and brackets outline 48 to 72 h comparisons. $^{\#\#}p < 0.01$ for comparison between WT and $EP3^{-/-}$ groups.

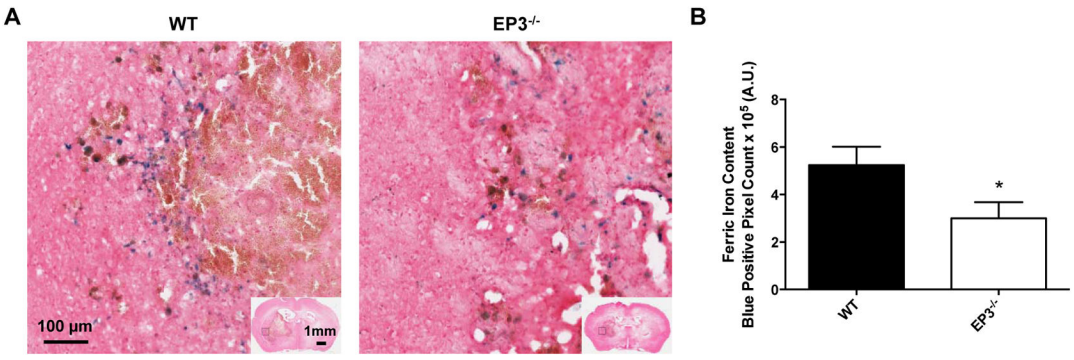

Fig. 3.

Genetic deletion of the PGE_2 EP3 receptor reduces brain ferric iron Perls' staining following ICH. At 72 h after ICH, Perls' staining of coronal brain sections from WT and $EP3^{-/-}$ mice was performed to evaluate ferric iron content. (A) Representative high magnification images showing ferric iron accumulation (blue) in perihematomal regions from WT (left) and $EP3^{-/-}$ mice (right). Square selections in the inserts denote magnified regions. (B) Blue positive pixel count analysis of the ipsilateral hemisphere showed that $EP3^{-/-}$ mice had significantly less ferric iron deposition (WT: n = 7, $EP3^{-/-}$: n = 8, *$p < 0.05$). No Perls' staining was seen in the contralateral hemisphere for any of the mice in the study.

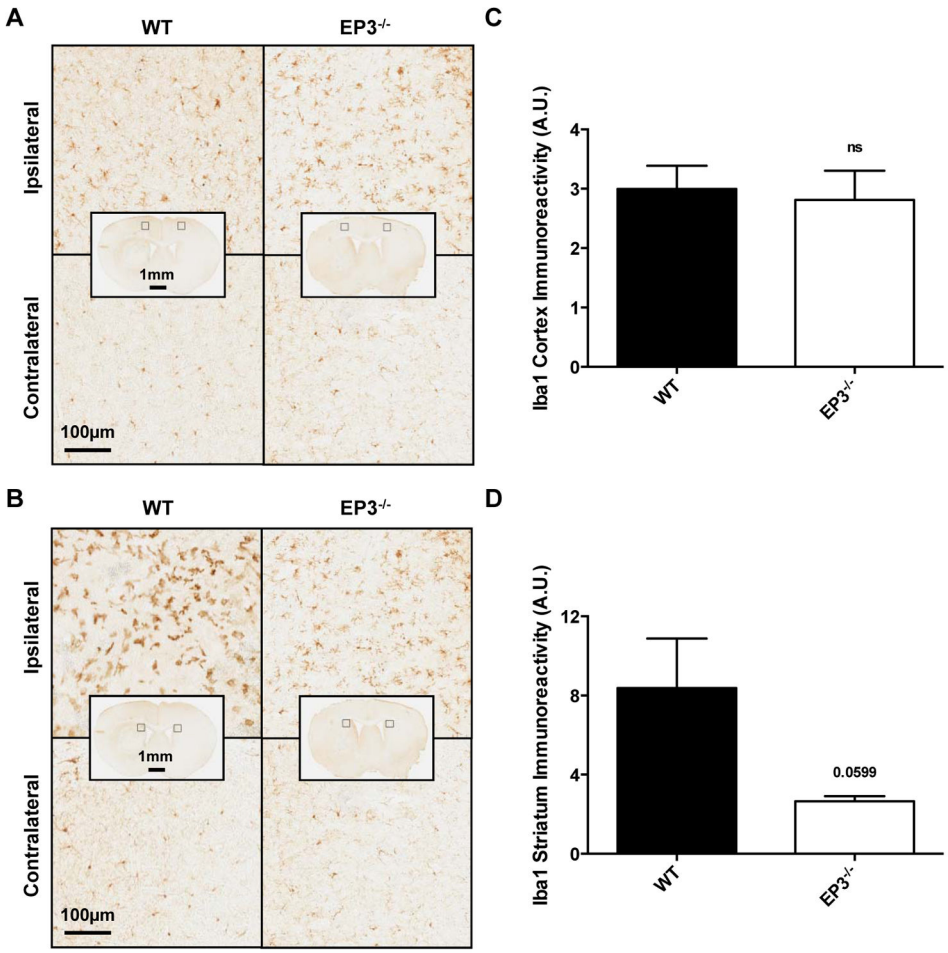

Fig. 4.

Effect of PGE_2 EP3 receptor deletion on microgliosis after ICH. Immunohistochemical staining for Iba1 was used to evaluate cortical and striatal microglial activation and morphological changes in WT and $EP3^{-/-}$ mice 72 h following ICH. (A and B) Representative high magnification images of coronal brain sections showing the ipsilateral and contralateral (A) cortex and (B) striatum for WT (left) and $EP3^{-/-}$ mice (right). Square selections in the inserts denote magnified regions. (C and D) Quantification of brown positive pixel count demonstrated that WT and $EP3^{-/-}$ mice had similar (C) cortical Iba1 immunoreactivity, whereas $EP3^{-/-}$ mice displayed less (D) striatal Iba1 immunoreactivity. This reduced striatal microglial activation was accompanied by less morphological changes. Data is normalized to the corresponding contralateral equivalent signal, with appropriate control for the area of quantification in striatal analyses (see methods). All comparisons included n = 7 WT and n = 6 $EP3^{-/-}$ mice and ns = not significant.

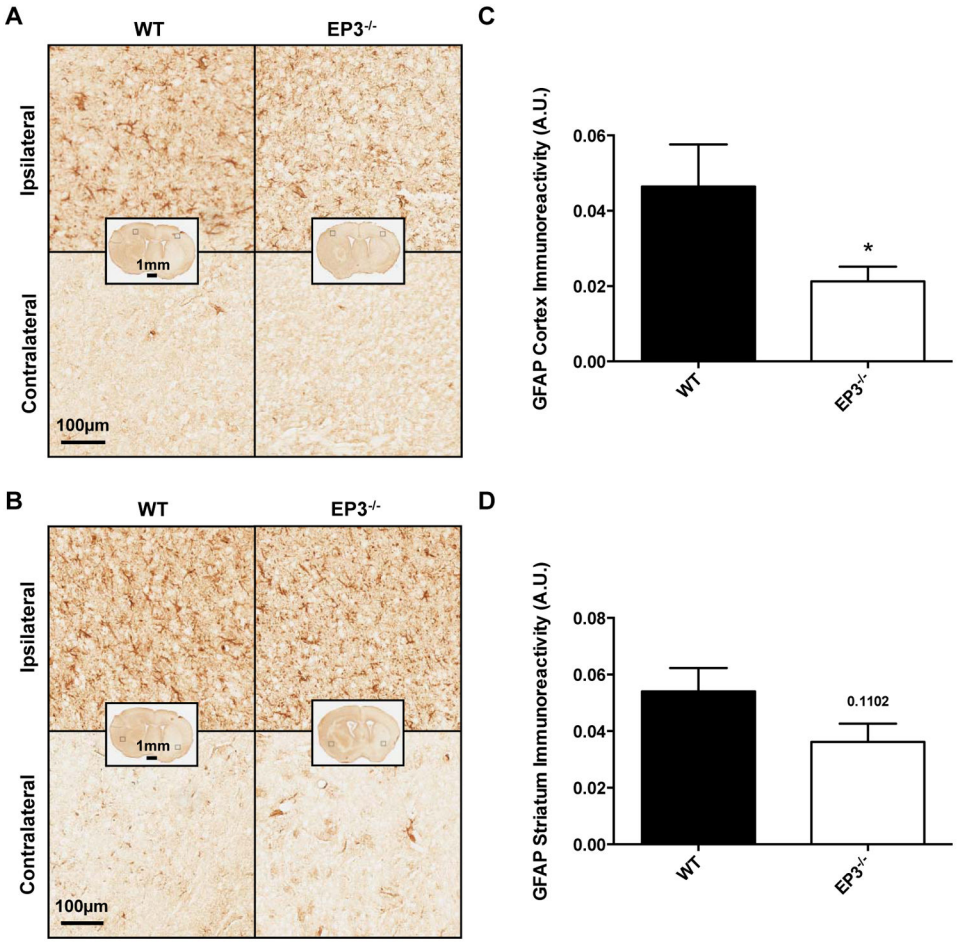

Fig. 5.

Effect of PGE_2 EP3 receptor deletion on astrogliosis after ICH. Immunohistochemical staining for GFAP was used to evaluate cortical and striatal astrogliosis in WT and $EP3^{-/-}$ mice 72 h following ICH. (A and B) Representative high magnification images of coronal brain sections showing the ipsilateral and contralateral (A) cortex and (B) striatum for WT (left) and $EP3^{-/-}$ mice (right). Square selections in the inserts denote magnified regions. (C and D) Quantification of brown positive pixel count demonstrated that $EP3^{-/-}$ mice had significantly reduced (C) cortical GFAP immunoreactivity, and tended to have less (D) striatal astrogliosis. Both groups demonstrated negligible staining in the contralateral cortex and striatum; thus, data is presented as ipsilateral immunoreactivity corrected for the area of quantification, without normalization for the contralateral equivalent (see methods and supporting information). All comparisons included n = 7 WT and n = 8 $EP3^{-/-}$ mice and *$p < 0.05$.

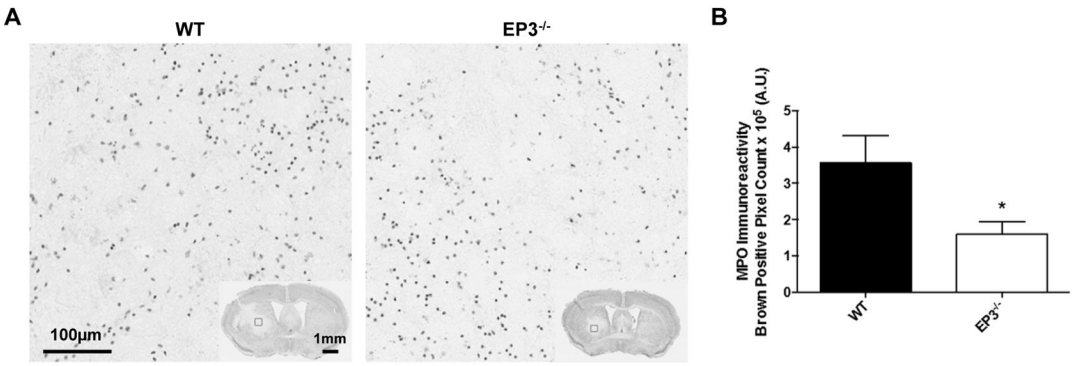

Fig. 6.

Genetic deletion of the PGE_2 EP3 receptor reduces peripheral neutrophil infiltration after ICH. Immunohistochemical staining for MPO was used to evaluate peripheral neutrophil infiltration in WT and $EP3^{-/-}$ mice 72 h following ICH. (A) Representative high magnification images of coronal brain sections showing MPO+ cells (brown) diffusely localized within injured brain regions. Square selections in the inserts denote magnified regions. (B) Brown positive pixel count analysis of the ipsilateral hemisphere showed that $EP3^{-/-}$ mice had significantly less peripheral neutrophil infiltration (WT: n = 5, $EP3^{-/-}$: n = 8, *$p < 0.05$). No MPO+ cells were seen outside of the injured brain areas for any of the mice in the study.

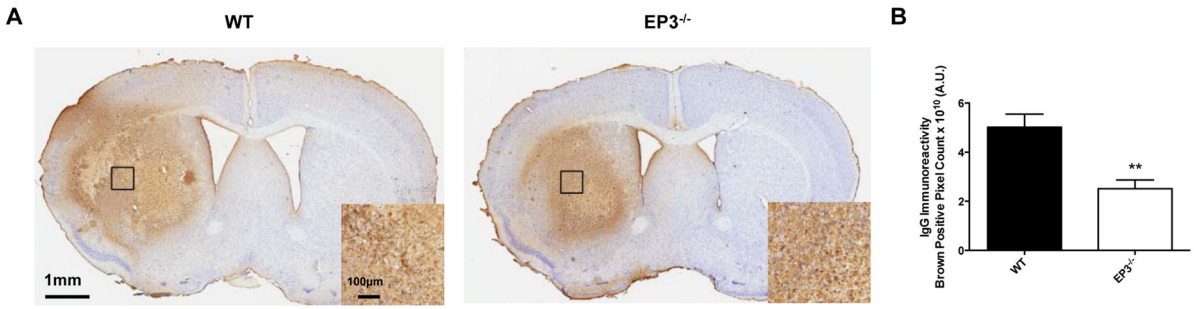

Fig. 7.

Genetic deletion of the PGE_2 EP3 receptor attenuates blood brain barrier breakdown after ICH. Immunohistochemical staining for mouse IgG was used to evaluate BBB breakdown in WT and $EP3^{-/-}$ mice at 72 h following ICH. (A) Representative images of coronal brain sections showing more disruption of the BBB in WT mice, which displayed a more diffuse staining pattern. Square boxes denote the location of high magnification inserts. (B) Whole brain brown positive pixel count analysis showed that $EP3^{-/-}$ mice had significantly reduced BBB breakdown (WT: n = 6, $EP3^{-/-}$: n = 7, **p < 0.01).